Synchronization of heterogeneous oscillator populations in response to weak and strong coupling

Dan Wilson,[1,a)] Sadegh Faramarzi,[2] Jeff Moehlis,[3] Mark R. Tinsley,[2] and Kenneth Showalter[2,b)]

[1]*Department of Electrical Engineering and Computer Science, University of Tennessee, Knoxville, Tennessee 37996, USA*

[2]*C. Eugene Bennett Department of Chemistry, West Virginia University, Morgantown, West Virginia 26506-6045, USA*

[3]*Department of Mechanical Engineering, University of California, Santa Barbara, California 93106, USA*

(Received 22 July 2018; accepted 19 November 2018; published online 14 December 2018)

Synchronous behavior of a population of chemical oscillators is analyzed in the presence of both weak and strong coupling. In each case, we derive upper bounds on the critical coupling strength which are valid for arbitrary populations of nonlinear, heterogeneous oscillators. For weak perturbations, infinitesimal phase response curves are used to characterize the response to coupling, and graph theoretical techniques are used to predict synchronization. In the strongly perturbed case, we observe a phase dependent perturbation threshold required to elicit an immediate spike and use this behavior for our analytical predictions. Resulting upper bounds on the critical coupling strength agree well with our experimental observations and numerical simulations. Furthermore, important system parameters which determine synchronization are different in the weak and strong coupling regimes. Our results point to new strategies by which limit cycle oscillators can be studied when the applied perturbations become strong enough to immediately reset the phase. *Published by AIP Publishing.*
https://doi.org/10.1063/1.5049475

Synchronization of limit cycle oscillators is of great interest in biology, as it plays a key role in the healthy functioning of cardiac pacemaker cells,[1] the genesis of circadian rhythms,[2,3] the development of neurological disease,[4,5] and the regulation of glucose through coordinated release of pancreatic insulin.[6] In this work, we carry out experiments and simulations on synchronization in populations of all-to-all photochemically coupled Belousov-Zhabotinsky oscillators, with the aim of developing theoretical strategies to predict synchronization in general populations of limit cycle oscillators. Analytical predictions agree well with numerical and experimental observations in the cases of weak and strong perturbations, where the system parameters predicting synchronization differ in each case.

I. INTRODUCTION

Winfree made great strides in describing the dynamical behavior of limit cycle oscillators,[7] with the critical insight that, near the limit cycle, the behavior of an M-dimensional oscillator could be understood in terms of a one-dimensional phase, resulting in dynamics given in the most general form by

$$\dot{\theta}_i = \omega_i + \frac{K}{N}\sum_{j=1}^{N} X_j(\theta_j)Z_i(\theta_i), \quad i = 1,\ldots,N. \qquad (1)$$

Here, $\theta_i \in [0, 2\pi)$ represents the phase of oscillator i, ω_i is its natural frequency, $Z_i(\theta)$ is the phase response curve to infinitesimal perturbations (iPRC), $X_j(\theta)$ is a phase-dependent influence function of oscillator j, and K sets the strength of coupling. While Eq. (1) provides a useful starting point for investigating populations of oscillators coupled through a mean field, it is difficult to study analytically. Various simplifications have been applied to Eq. (1) that have resulted in increased analytical tractability. Perhaps the most well-known simplification is the Kuramoto model,[8] for which $X_j(\theta_j)Z_i(\theta_i)$ is replaced by $\sin(\theta_j - \theta_i)$. The resulting model can be further simplified in the limit as $N \to \infty$, allowing it to be succinctly described in terms of the evolution of the probability densities of oscillators. The balance between complexity and analytical tractability of the Kuramoto model has sparked much interest over time, providing significant insights into the spontaneous synchronization of coupled oscillators.[9–13]

Other strategies have been used to shed light on the synchronization of coupled oscillators. For example, the notion of a master stability function can be used to determine the stability of synchronous solutions of identical oscillators with linear coupling and general connectivity.[14,15] Contraction theory[16,17] provides a strategy for guaranteeing synchronization in general populations of oscillators, provided a contraction region can be found, although the implementation of this methodology is not always straightforward, particularly for large and complicated systems. By assuming that all oscillators have an identical natural frequency and communicate through brief pulses, it is possible to investigate the long-term behavior of a population of oscillators starting from an arbitrary set of initial conditions.[18,19] Various constraints on the iPRC or influence function of Eq. (1) have been considered, making it possible to investigate complicated behavior such as oscillator death and chimera states.[20,21]

a)Electronic address: dwilso81@utk.edu
b)Electronic address: kshowalt@wvu.edu

Few practical tools exist for answering basic questions about the stability of synchronized oscillations for heterogeneous populations of limit cycle oscillators. In this work, using synchronization in populations of all-to-all photochemically coupled Belousov-Zhabotinsky (BZ) oscillators as a test bed, we develop strategies to predict synchronization in general populations that can be described by the Winfree model, Eq. (1). The first strategy assumes that perturbations due to coupling are sufficiently weak that they can be characterized by an iPRC, and we draw on graph theoretical techniques to develop sufficient conditions for synchronization of a heterogeneous population of oscillators in this instance. The second strategy is applicable for stronger coupling, for which perturbations give rise to nearly immediate resetting of the phase to zero; we make use of a phase dependent spike threshold curve (STC) in order to predict stable synchronization in this regime. These strategies are assessed in terms of their ability to predict the critical coupling strength, defined as the minimum coupling strength for which the synchronized state is stable. In both cases, analytical predictions agree well with numerical and experimental observations. Furthermore, we find that important system parameters determining synchronization and the qualitative behavior of the synchronized solutions are different for each regime. The results presented here have direct implications to the understanding of general populations of biological oscillators and point to new opportunities for study where our understanding is incomplete.

II. EXPERIMENTS AND NUMERICAL SIMULATIONS

To study the collective behavior of populations of coupled oscillators, experiments are carried out using discrete photosensitive BZ chemical micro-oscillators. The BZ reaction is a multi-step oscillatory reaction involving the acidic bromate oxidation of an organic compound such as malonic acid in the presence of a metal catalyst such as ruthenium(II). In our experiments, we used catalyst loaded cation exchange beads with an average diameter of 270 μm, which are placed in a catalyst-free BZ reaction mixture.[22–26] The catalyst changes color from green to orange, corresponding to its oxidized and reduced states, respectively. The accompanying gray level changes allow the measurement of the natural period of a given oscillator. We define $\theta_i = 0$ to be the moment that the measured gray level intensity reaches its maximum value for each oscillator, corresponding to the maximum concentration of the oxidized catalyst, which permits calculation of the period. The phase θ_i at any point in time can then be determined.

Phase response curves (PRCs) can be measured using the well established direct method[27] by briefly raising the background light intensity ρ_0 by some amount $\Delta\rho$ for Δt seconds and measuring the difference between the expected and actual time of the next spike $\Delta\theta$. We take the iPRC at that phase to be equal to $\Delta\theta/(\Delta\rho\Delta t)$. The BZ reaction provides a particularly interesting test bed for the study of the Winfree model, because, depending on the magnitude of stimulation, the individual oscillators can fire virtually immediately. Figure 1(a) shows a typical phase response curve, in this case with a light perturbation of 0.64 mW cm^{-2}. There is a small downward trend until $\theta \approx 2.5$ rad, at which point the perturbation results in the oscillator firing, with nearly immediate phase resetting to $\theta = 0$.

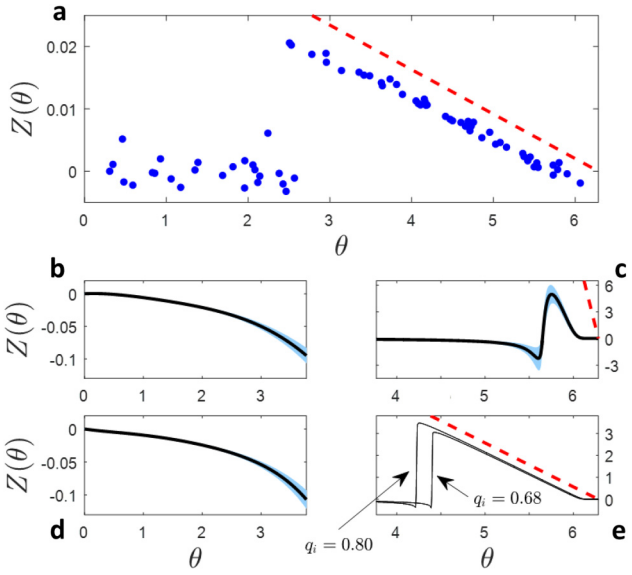

FIG. 1. Measured phase response curves in the experimental BZ system and numerical simulations using the ZBKE model. Panel (a) shows an example of $Z(\theta)$ measured in a BZ experiment with perturbations of 0.64 mW cm^{-2}. Dots give individual measurements from the direct method.[27] Panels (b) and (c), and (d) and (e) show simulations with perturbations $\Delta\rho$ of magnitude 0.05 and 1.0, respectively. For larger perturbations, nearly immediate phase resetting is observed once the phase is large enough. Light blue bands give the envelope of phase response curves measured for the heterogeneity $q \in [0.68, 0.80]$, with the black line showing the average between these bounds. In panels (a), (c), and (e), the dashed red lines indicate the upper bound which would be achieved with an instantaneous reset to $\theta = 0$. In panel (e), immediate phase resetting occurs for smaller values of θ as values of q_i increase.

Numerical simulations of the BZ chemical micro-oscillator system are carried out with a two-variable, nondimensional version of the Zhabotinsky-Buchholtz-Kiyatkin-Epstein (ZBKE) model,[28] modified to incorporate the photosensitivity of the ruthenium catalyzed discrete oscillator[22]

$$\begin{aligned}\epsilon_1\dot{x}_i &= \rho_i/2\chi - x_i^2 - x_i + \epsilon_2\lambda u_{ss}^2 + u_{ss}(1-z_i)\\ &\quad + \frac{\mu - x_i}{\mu - z_i}\left(\frac{q_i\alpha z_i}{\epsilon_3 + 1 - z_i} + \eta\right),\\ \dot{z}_i &= \rho_i/\chi + u_{ss}(1-z_i) - \frac{\alpha z_i}{\epsilon_3 + 1 - z_i}, \quad i = 1,\ldots,N.\end{aligned} \tag{2}$$

Here, N is the total number of oscillators, q_i is the stoichiometric coefficient, x_i and z_i represent $[HBrO_2]$ and $[Ru(bpy)^{3+}]$ for oscillator i, respectively, model parameters $\epsilon_1 = 0.11$, $\epsilon_2 = 1.7 \cdot 10^{-5}$, $\epsilon_3 = 1.6 \cdot 10^{-3}$, $\lambda = 1.2$, $\alpha = 0.1$, $\eta = 1.7 \cdot 10^{-5}$, $\chi = 500$, and $\mu = 2.4 \cdot 10^{-4}$, and ρ_i represents the illumination intensity of oscillator i for the photochemical coupling, with $\rho_0 = 0.54$ as the background light intensity. The variable u_{ss} represents the steady-state $[HBrO_2^+]$ and for oscillator i is determined according to $u_{ss} = [1/(4\lambda\epsilon_2)][-(1-z_i) + (1 - 2z_i + z_i^2 + 16\lambda\epsilon_2 x_i)^{0.5}]$.

The original ZBKE model[28] involved the three variables $HBrO_2$, $HBrO_2^+$, and oxidized catalyst (ferroin or cerium) with the quasi steady state approximation (QSSA) applied to a fourth variable bromide, Br^-. A two variable version

of this model was introduced by Bugrim *et al.*[29] in which both $HBrO_2^+$ and Br^- were represented using a QSSA. This two-variable model was later modified for use with the photosensitive BZ system with the $Ru(bpy)_3^{2+}$ catalyst by Vanag *et al.*[30]

The ZBKE model has been used widely in studies of coupled micro-oscillators, in part due to the fact that it can reproduce the range of frequency heterogeneity seen in such systems. Toth *et al.*[31] used a three variable version of the ZBKE with the variables $HBrO_2$, Br^-, and oxidized catalyst (ferroin) and the QSSA applied to the fourth species $HBrO_2^+$ to study micro-oscillators coupled via a well stirred catalyst-free solution. In this system, the micro-oscillators communicate mainly through the interchange of bromous acid and bromide. This model was also utilized in a study of dynamical quorum sensing in large populations of chemical oscillators.[32] The two variable model of Vanag *et al.*[30] was first applied to photosensitive micro-oscillators coupled via light by Taylor *et al.*[22] This version of the model has since been extensively used in studies of coupled light sensitive micro-oscillators.[24–26,33–38] The model utilizes coupling based on the transmitted light intensity from each oscillator and, from this, each oscillator is irradiated with a calculated light intensity. The experimental micro-oscillators are spatially separated so that there is no diffusive coupling between them.

The dimensionless modified ZBKE model in Eq. (2) is intended to provide a numerical analog to the experimental system. While the behavior between different models is qualitatively similar, quantitative comparisons between most model simulations of the Belousov-Zhabotinsky reaction and experimental results typically have not been possible. As such, the experimental results and the numerical simulations in this work are analyzed separately, each yielding comparable behavior that can be explained using the same theoretical approach described below.

Figures 1(b) and 1(c) show simulated phase response curves measured for $q \in [0.68, 0.80]$ and a perturbation in the excitatory feedback of $\Delta\rho_i = 0.05$, lasting $\Delta t = 0.5$. The infinitesimal phase response curve is measured for these small perturbations, which varies smoothly as the phase of the stimulus application changes. For larger perturbations of $\Delta\rho_i = 1.0$ with $\Delta t = 0.5$, we measure a nearly identical phase response curve at smaller phases, but observe nearly immediate phase resetting when $\theta > 4.3$ rad, as shown in Figs. 1(d) and 1(e).

The qualitative differences in the response to perturbations (i.e., infinitesimal phase response vs. nearly immediate phase resetting) result in profound differences in the synchronization of oscillator populations, as can be observed in populations of coupled BZ oscillators. For each experiment, 40 micro-oscillators were placed in a petri dish containing 2.5 ml of catalyst-free BZ solution, with minimum spacing of 1.0 mm between the oscillators. The oscillators are coupled by monitoring the gray level of each oscillator with a CCD camera and applying the appropriate feedback light intensity with a spatial light modulator (SLM).[24–26] Figure 2 shows a schematic representation of the experimental setup.

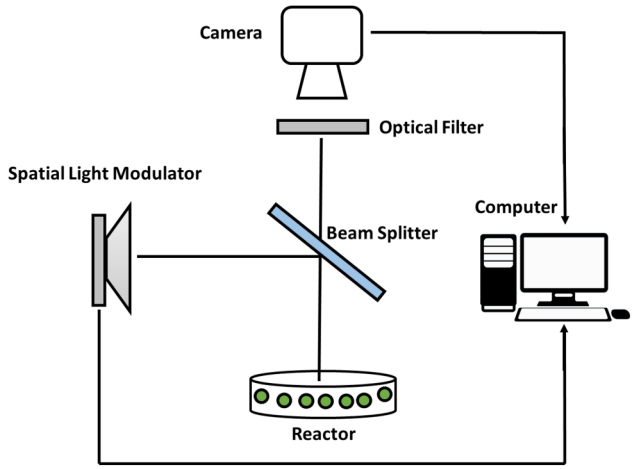

FIG. 2. Experimental setup for studies of synchronization of coupled BZ micro-oscillators according to Eq. (3). The gray levels I_i and I_j of the photosensitive micro-oscillators are monitored with a CCD camera and the illumination feedback ρ_i^e is applied with a spatial light modulator (SLM), where ρ_0^e is the background illumination intensity.

The light intensity, ρ_i^e (mW cm^{-2}), projected on oscillator i in the experiments is determined by

$$\rho_i^e = \rho_0^e + \frac{K}{N}\sum_{j\neq i}[I_j(t-\tau) - I_i(t)], \tag{3}$$

where $N = 40$ is the total number of oscillators, K is the coupling constant (mW cm^{-2}), I_i and I_j are the normalized, dimensionless gray levels of oscillators i and j, t is the time (s), τ is a time delay (s), and ρ_0^e is the background light intensity (mW cm^{-2}). As evident from (3), the experimental oscillators are connected in an all-to-all manner without self coupling. The purpose of including the time delay is twofold: First, non-negligible time delays are often observed in biological systems, a feature which has been precisely quantified and studied in neurological systems.[39,40] Second, the manipulation of τ allows us to modify the system so that the feedback occurs earlier or later in the cycle during synchronization. This permits us to study different mechanisms of synchronization by determining whether the behavior can be captured by an iPRC or by the STC for larger perturbations displaying nearly immediate phase resetting. For example, consider the order parameter plots shown in Figs. 3(b) and 3(d) from experiments using the coupling in Eq. (3), with $\tau = 6$ s and $\tau \in \{50, 60\}$ s, respectively. In these experiments, the coupling strength is initially set to a sufficiently high value so that the oscillators completely synchronize, at which point the coupling constant K is set to a particular value and the steady state Kuramoto order parameter,[8] $R = |(1/N)\sum_{k=1}^{N} e^{i\theta_k}|$, is recorded, yielding plots of R as a function of K.

The average natural period of the oscillators in our experiments is approximately 66 s, so that when the oscillators are synchronized, most of the effective feedback occurs later in the cycle due to the rapid upstroke and decay of the gray scale intensity, as shown, for example, in Figs. 3(e) and 3(f). For short time delays, we observe a clear trend emerging in the plots of R as a function of K, with a reasonably tight distribution in the values of R. For larger values of τ, provided K is large

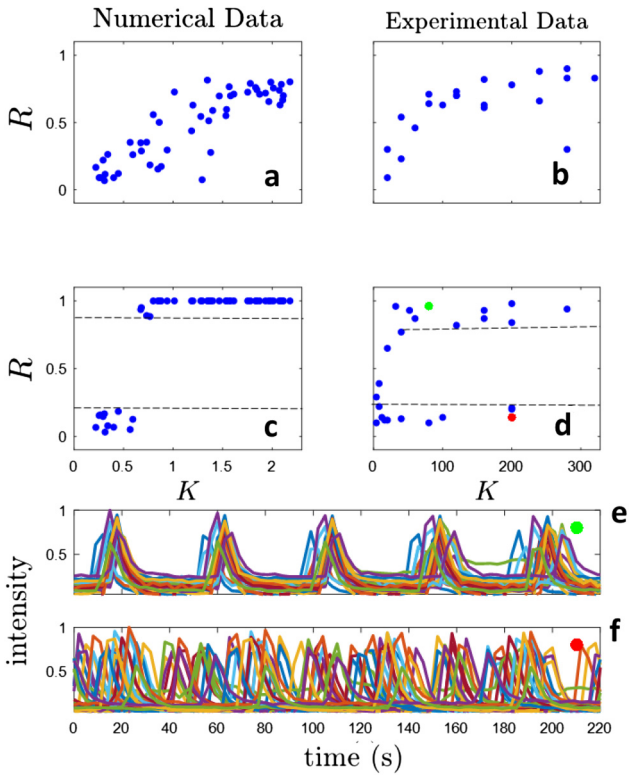

FIG. 3. Panels (a) and (c) show plots of long-time values of the order parameter R as a function of coupling strength K for simulations using Eq. (2) with coupling given by Eq. (4) for $\tau \approx 17\%$ and 82% of the natural period, respectively. Panels (b) and (d) show similar results from experimental preparations of the BZ chemical reaction with τ set to approximately 9% and 83% of the natural period, respectively. For τ values that are a larger percentage of the natural period, R generally takes a value that is very close to either 1 or 0 and dashed lines in panels (c) and (d) highlight this dichotomy. Panels (e) and (f) show long-time behavior of each oscillator from experiments corresponding to the data points of matching color in panel (d). Intensities shown are normalized with respect to their maximum value.

enough, we observe a clear all-or-nothing synchronization, which does not depend strictly on K. Figures 3(e) and 3(f) show time series of the oscillators corresponding to the data points of matching color in Fig. 3(d). Notice that even though the coupling strength in Fig. 3(f) is more than twice that in Fig. 3(e), the asymptotic behavior of the system is completely incoherent. Reasons for this discrepancy will be discussed in the numerical and analytical results to follow.

Qualitatively similar behavior is observed in simulations of Eq. (2), with coupling given by

$$\rho_i = \rho_0 + \frac{K}{N}\sum_{j=1}^{N}[z_j(t-\tau) - z_i(t)] \tag{4}$$

for $t \geq 0$, where $\rho_0 = 0.54$, $N = 40$, and the concentrations of the oxidized catalyst z_i and z_j are assumed to be proportional to the transmitted light intensities I_i and I_j so that Eq. (4) is an analog of Eq. (3). However, like Eq. (2), all quantities in Eq. (4) are dimensionless. Unlike in experiments, oscillators in numerical simulations do have self coupling. However, there is no discernable difference between simulations with or without self coupling with $N = 40$. In each simulation, the value of q in Eq. (2) is chosen from a Gaussian distribution with a mean of 0.7 and a variance chosen randomly before each trial between 0 and 0.1; the resulting uncoupled periods averaged 34. In order to obtain a sufficient history to implement the coupling in Eq. (4) with time delay τ, Eq. (2) is initially paced when $t < 0$ using $\rho_i = \rho_0 + \kappa$ where $\kappa = 1$ if $\mathrm{mod}(t, 30) < 0.5$ and $\kappa = 0$ otherwise. This pacing is strong enough to elicit immediate spikes and initially synchronizes all oscillators. Simulations are performed using a forward Euler scheme with a time step of 0.001 time units.

Each oscillator initially has the same state, and the order parameter is recorded once the system achieves its long-time behavior. Similar to the experimental data, when $\tau = 6$ as in Fig. 3(a), we observe a clear positive and smoothly varying trend in R as a function of K. For $\tau = 28$ [Fig. 3(c)], we observe an abrupt transition between complete incoherence and complete synchronization. Furthermore, upon synchronization, the order parameter remains near the perfectly synchronized state with $R = 1$, a level of synchronization that is never achieved for small τ.

III. ANALYSIS OF TWO DIFFERENT MODALITIES OF SYNCHRONIZATION

In Fig. 3, we observe qualitative differences in synchronization when τ is a small fraction [Figs. 3(a) and 3(b)] or large fraction [Figs. 3(c) and 3(d)] of the unperturbed natural period. As mentioned earlier, these differences are due to the dichotomy of behavior based on whether perturbations arrive at smaller values of θ, with behavior that can be described with an infinitesimal phase response curve, or at large values of θ, with virtually immediate phase resetting behavior.

To study synchronization, we must first give a technical definition of what it means for a population of oscillators to be synchronized. Here, we will use the notions of *frequency synchronization* and *phase cohesion*[41] to study the behavior of these populations of coupled oscillators analytically. We will say that a solution to Eq. (1) is phase cohesive at time t^* if there exists $\gamma \in [0, \pi)$ such that for all θ_i and for all $t \geq t^*$, an arc length γ can be found that contains all θ_i. Frequency synchronization is achieved at time t^* if $\dot{\theta}_i(t) = \dot{\theta}_j(t)$ for all i and j for all times $t \geq t^*$. Figure 4 illustrates the qualitative differences between these two definitions of synchronization. Note that frequency synchronization does not necessarily imply phase cohesiveness. For example, the splay state can be frequency synchronized but not phase cohesive.

The critical coupling strength, K_c, defined as the necessary and sufficient coupling strength that will maintain either phase cohesiveness or frequency synchronization, is often used to quantify the relevant parameters that determine synchronization. In special cases for a given population, one can determine K_c analytically, but in most applications, K_c can only be determined directly through experiment or direct numerical simulation. In the subsections to follow, we derive an upper bound on K_c for a heterogeneous population in Eq. (1), valid in the limit of weak coupling when the population has both a heterogeneous distribution of natural frequencies and infinitesimal phase response curves. As we will show, this bound is applicable in experimental preparations of the BZ reaction and in simulations of Eq. (2) when τ from Eqs. (3) and (4) is a small fraction of the natural period.

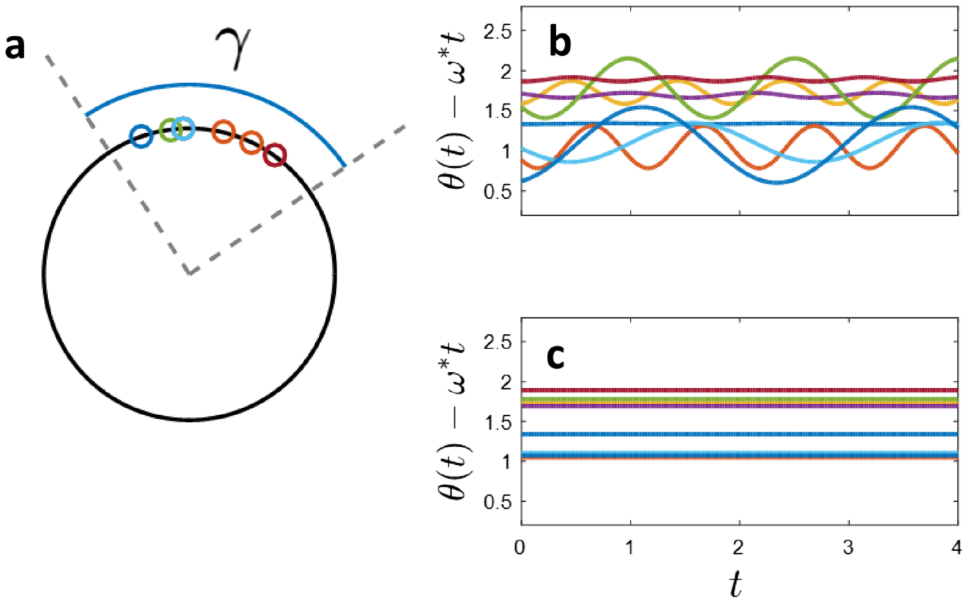

FIG. 4. In panel (a), a general system of 8 oscillators from Eq. (1) has phases which are contained within an arc of length γ at a snapshot in time. In panels (b) and (c), ω^* is a constant so that each trace is plotted in a rotating reference frame. The example population in panel (b) is phase cohesive, even though the relative position of each oscillator changes. In panel (c), the example population is frequency synchronized, and all oscillators travel at the rate ω^*.

We also derive an upper bound on K_c for phase cohesion when the system behavior is dominated by immediate phase resetting, as is the case when τ is a larger proportion of the natural period. As we will show, for the two different modalities of synchronization, the relevant parameters which determine synchronization in Eq. (1) are different.

A. Infinitesimal phase reseting critical coupling bounds

Here, we examine synchronization in Eq. (1) in the limit of weak coupling, i.e., when $Z(\theta)$ can be approximated by an infinitesimal phase response curve. The theoretical analysis in Sec. III A also appears in Ref. 45. To begin, consider a weakly forced population of oscillators, each with a stable limit cycle

$$\dot{x}_i = F(x_i) + \epsilon G_i(t), \quad x_i \in \mathbb{R}^M, \quad i = 1, \ldots, N, \tag{5}$$

where x_i is a state vector, $G_i \in \mathbb{R}^M$ represents an external perturbation, and $0 < \epsilon \ll 1$. For simplicity, we will take $G_i(t) = [u_i(t), 0, \ldots, 0]^T$ so that perturbations are applied only to a single state variable. In the limit that external perturbations are small, Eq. (5) is well approximated in phase reduced form[27,42]

$$\dot{\theta}_i = \omega_i + \epsilon Z_i(\theta_i) u_i(t), \quad i = 1, \ldots, N, \tag{6}$$

where θ_i is the phase of oscillator i, giving its location in phase space with respect to its limit cycle ζ_i, ω_i is the natural frequency of oscillator i, N is the number of oscillators, $Z_i(\theta_i)$ is the infinitesimal phase response curve (iPRC) of oscillator i, which describes the phase change associated with a small perturbation, and $u_i(t)$ is a general external perturbation to oscillator i. In the analysis to follow, we will assume that when perturbations are sufficiently small, each oscillator remains order ϵ close to ζ_i. This implies that to leading order ϵ, there is a one-to-one correspondence between the phase and the system's state variables, i.e., $x_i(\theta_i) = \zeta_i(\theta_i) + \mathcal{O}(\epsilon)$. The formulation in Eq. (6) allows the population to have both significantly different phase response curves and natural frequencies.

To analyze synchronization in the chemical oscillator network, suppose that the feedback coupling is all-to-all with self coupling so that $u_i(t)$ takes the form

$$u_i(t) = -\frac{K}{N}\sum_{j=1}^{N} c(x_i, x_j) = -\frac{K}{N}\sum_{j=1}^{N} f(\theta_i, \theta_j) + \mathcal{O}(\epsilon). \tag{7}$$

Here, $K > 0$, c is a function of the state of each oscillator, and f can be determined by evaluating c on a given oscillator's limit cycle. With these assumptions, we rewrite (6) to leading order ϵ as

$$\dot{\theta}_i = \omega_i - \epsilon Z_i(\theta_i)\left[\frac{K}{N}\sum_{j=1}^{N} f(\theta_i, \theta_j)\right]. \tag{8}$$

Note that $f(\theta)$ is a 2π periodic function in both θ_i and θ_j. We manipulate Eq. (8) by letting $\phi_j \equiv \theta_j - \omega_o t$, $\phi_i \equiv \theta_i - \omega_o t$, and $\varphi_{i,j} \equiv \phi_i - \phi_j$, with ω_o corresponding to the mean natural frequency of the oscillators, to arrive at the relation

$$\dot{\phi}_i = \Delta\omega_i - \frac{\epsilon K}{N}\sum_{j=1}^{N} Z_i(\varphi_{i,j} + \phi_j + \omega_o t) f(\varphi_{i,j} + \phi_j + \omega_o t, \phi_j + \omega_o t). \tag{9}$$

Here, $\Delta\omega_i \equiv \omega_i - \omega_o$. Noting that Eq. (9) is T-periodic, with $T = 2\pi/\omega_o$, its dynamics can be approximated using averaging theory[43,44]

$$\begin{aligned}\dot{\vartheta}_i &= \frac{1}{T}\int_0^T \Big[\Delta\omega_i - \frac{\epsilon K}{N}\sum_{j=1}^{N} Z_i(\varphi_{i,j} + \phi_j + \omega_o t) f(\varphi_{i,j} + \phi_j + \omega_o t, \phi_j + \omega_o t)\Big] dt \\ &= \Delta\omega_i - \underbrace{\frac{K}{N}\int_0^T \frac{\epsilon}{T}\left[\sum_{j=1}^{N} Z_i(\varphi_{i,j} + \omega_o t) f(\varphi_{i,j} + \omega_o t, \omega_o t)\right] dt}_{\Gamma_i(\varphi_{i,j})}.\end{aligned} \tag{10}$$

Note that in the second to last line of (10), ϕ_j can be neglected because it is common to all terms in the T-periodic integrand. Here, $\Gamma_i(\varphi_{i,j})$ represents the averaged total phase difference coupling for oscillator i. Provided the terms in the right hand side of (9) are small enough, $\dot{\vartheta}_i$ will be a good approximation of $\dot{\phi}_i$. Toward determining a bound for the critical coupling strength for synchronization in (10), consider the following conditions for some $\gamma \in (0, \pi)$:

(I) For all i and j, $\min_{a\in[0,\gamma]}\left[\Gamma_i(a) - \Gamma_j(a-\gamma)\right] \geq (\omega_{\max} - \omega_{\min})/K$.
(II) For all i, there exists $\delta_i > 0$ such that when $-\gamma \leq \varphi \leq \gamma$, $\frac{d}{d\varphi}\Gamma_i(\varphi) > \delta_i$.

The main results for synchronization for populations of oscillators in response to weak coupling are given below, with a proof given in Appendix A. A proof of these statements is also given in Ref. 45.

Sufficient condition for phase cohesion: If (I) is satisfied, then for some initial time t_0 for which $\max_{i,j}|\vartheta_i(t_0) - \vartheta_j(t_0)| \leq \gamma$, it follows that $|\vartheta_i(t) - \vartheta_j(t)| \leq \gamma$ for all $t > t_0$.

Sufficient condition for frequency synchronization: If (I) and (II) are satisfied, then for some initial time t_0 for which $\max_{i,j}|\vartheta_i(t_0) - \vartheta_j(t_0)| \leq \gamma$, the network (10) is exponentially frequency synchronized.

We note that the results above are only valid for the averaged system equation (10). However, if the inter-oscillator coupling is small enough, then ϑ_i is well approximated by θ_i. If additionally the averaged equation (10) achieves stable frequency synchronization, then the unaveraged equation (8) will have an associated stable periodic orbit when the coupling is small enough, as discussed in Refs. 43 and 44.

Keeping condition (I) in mind, one can verify the following upper bound on K_c, the critical coupling strength for phase cohesion in the network

$$K_c \leq \frac{\omega_{\max} - \omega_{\min}}{\beta},$$
$$\beta = \max_{\gamma\in(0,\pi)}\left[\min_{a\in[0,\gamma]}\left[\Gamma_{\min}(a) - \Gamma_{\max}(a-\gamma)\right]\right]. \quad (11)$$

The upper bound equation (11) may appear onerous at first glance but is straightforward to calculate after $\Gamma_{\min}$ and $\Gamma_{\max}$ have been determined using the strategy presented in Appendix B. Furthermore, the constant β can be calculated without explicit knowledge of any of the iPRCs but rather using a range within which iPRCs can be found. This feature is useful, for instance, in biological systems[46] when the measurement of individual phase response curves is not possible. Intuitively, β gives a sense of the guaranteed synchronizing influence from weak coupling which explicitly takes into account system heterogeneity. While Eq. (11) only provides an upper bound, in general, one would expect K_c to decrease as β increases. Finally, we note that it is relatively straightforward to adapt the resulting bound (11) for situations when the network does not have self coupling.

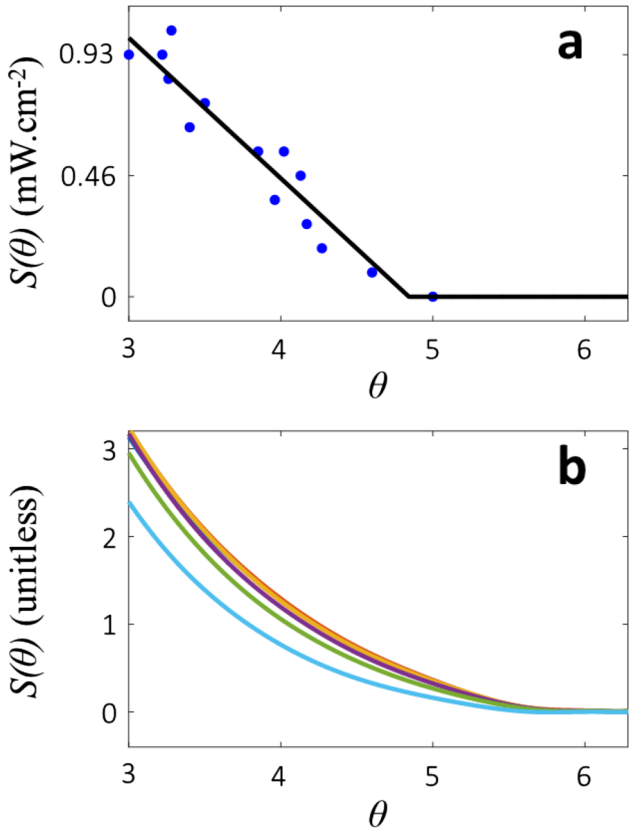

FIG. 5. (a) Blue dots represent individual measurements of $S(\theta)$ for BZ experiments using the procedure detailed in the text. The solid line gives a piecewise linear fit to the data. (b) $S(\theta)$ is calculated for oscillators from simulations of Eq. (2), with $q_i = \{0.500, 0.574, 0.648, 0.722, 0.796, 0.870\}$.

B. Spike threshold resetting and synchronization

We require a different mathematical formalism to study synchronization when τ is a larger fraction of the natural period in the BZ oscillator experiments. For large τ, perturbations due to coupling occur near the end of the cycle in a fully synchronized system. As illustrated in Fig. 1(a), for perturbations of a given magnitude, when the perturbation is applied for sufficiently large θ, we observe a nearly immediate spike, which resets the phase to $\theta = 0$. In Fig. 5(a), we observe that this threshold shifts to smaller phases as the intensity of the stimulus increases.

Each experimental data point in Fig. 5(a) is obtained by carrying out a PRC measurement with a light perturbation. The light perturbation is applied for 6 s to all oscillators and the phase difference, $\Delta\theta$, is measured for each oscillator. The oscillators are allowed to relax for at least 2 periods before the next perturbation. Finally, all values of $\Delta\theta$ for all oscillators are collected and plotted as a function of the phase at which they are perturbed. Figure 5(a) shows the individual PRC experiments with changing the maximum light intensity, $S(\theta)$, by increments of 0.093 mW cm^{-2}. The x-axis represents the minimum phase at which immediate resetting to $\theta = 0$ occurs. As seen in Fig. 5(a), θ shifts toward lower values as $S(\theta)$ increases.

The plot of the experimental data in Fig. 5(a) appears nearly linear, and we fit the data to the piecewise linear curve to determine a spike threshold curve (STC) denoted

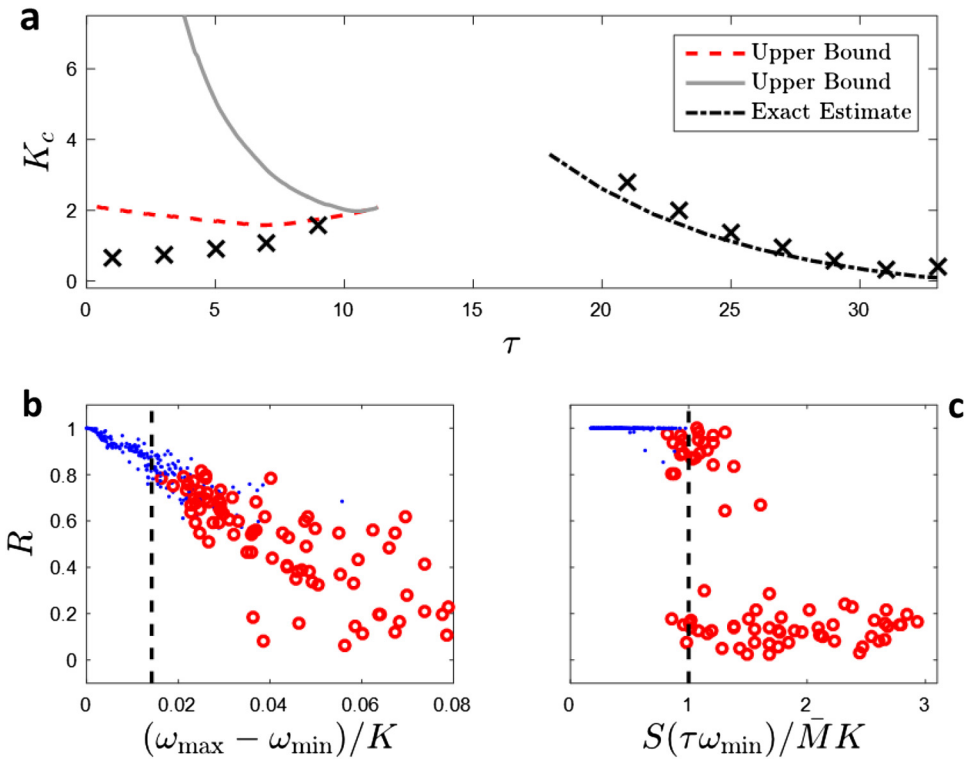

FIG. 6. (a) Crosses represent numerically determined values of K_c in simulations of Eq. (2). The solid line gives an upper bound calculated using the iPRC, Eq. (11). The dashed line gives an upper bound, taking into account the low threshold for producing a spike near the end of the oscillation in the ZBKE system. The dashed-dotted line gives an exact estimate for K_c using Eq. (14). (b) and (c) Plots of R versus the relevant parameters that determine synchronization. Simulations in panel (b) [respectively, (c)] use $\tau = 6$ time units (respectively, $\tau = 28$ time units), resulting in synchronization that is best predicted using infinitesimal phase resetting (respectively, immediate phase resetting). Dashed lines are calculated according to Eqs. (11) and (14) and represent cutoff values for synchronization in the system. Closed and open circles represent simulations that remain phase cohesive and lose phase cohesiveness, respectively.

by $S(\theta)$. In experimental trials, any measurable increase in light intensity when $\theta > 5$ elicits a nearly immediate spike, and we take $S(\theta) = 0$ in this regime. Numerical simulations of Eq. (2) yield qualitatively similar results, and $S(\theta)$ is determined numerically with a shooting method for six oscillators with different values of q_i. The lowermost curve (respectively, topmost curve) in panel (b) gives the trace calculated for $q_i = 0.87$ (respectively, $q_i = 0.50$), with the remaining curves representing intermediate values.

In both simulations and experiments, the STC can be interpreted as follows: any perturbation P for which $P \geq S(\theta)$ will elicit an almost immediate spike; when $P < S(\theta)$, the perturbation falls in a regime that can be characterized by an iPRC. For a synchronous population of oscillators for which τ is close to the natural period of oscillation, perturbations due to feedback occur primarily in this immediate phase resetting regime. Notice from the phase response curves shown in Fig. 1 that perturbations for which $P \geq S(\theta)$ generally have a much greater effect on the phase than perturbations for which $P < S(\theta)$. For this reason, we will ignore the effects of the iPRC in the analysis to follow and focus on the STC in determining thresholds to maintain synchronization.

To proceed with the analytical derivation of the critical coupling strength, suppose the coupling takes the form given by Eq. (7). Feedback will produce an immediate spike in oscillator i provided that the following holds:

$$\frac{K}{N}\sum_{j=1}^{N} f(\theta_i, \theta_j) > S_i(\theta_i), \tag{12}$$

where S_i represents the STC of oscillator i. The following assumptions will be used to calculate K_c in this regime. First, suppose Eq. (8) is initially synchronized with all spikes occurring at the same instant, i.e., $\theta_i = 0$ at $t = t_0$ for all i. Recall that $\theta_i = 0$ corresponds to the moment that oscillator i reaches its maximum gray level value. From the coupling, the resulting spike will be felt by other oscillators at $t = t_0 + \tau$. We find that in both numerical simulations and experiments, the baseline intensities between oscillators are effectively similar, but the maximum value of the intensities varies between oscillators. Therefore, we will define M_j as the maximum value of $f(\theta_i, \theta_j)$ (i.e., the difference between the maximum intensity of oscillator j and baseline intensity of oscillator i). Furthermore, feedback ramps up quickly and decays rapidly; we assume that coupling either elicits a spike at $t = t_0 + \tau$ or is not sufficient to cause a premature spike. Taken together, we can guarantee that the system will remain synchronized, i.e., coupling will be strong enough to elicit spikes in all oscillators at the same time, provided

$$K > \max_i \left[S_i(\tau\omega_i)\right]/\bar{M}, \tag{13}$$

where $\bar{M} \equiv (1/N)\sum_{j=1}^{N} M_j$. Equation (13) can be used to bound the critical coupling strength to maintain synchronization,

$$K_c \leq S_{\max}(\tau\omega_{\min})/\bar{M}, \tag{14}$$

where $S_{\max}(\theta) \equiv \max_i[S_i(\theta)]$. In Eq. (14), we use the fact that $S(\theta)$ is monotonically decreasing so that the slowest oscillator determines the coupling strength required for synchronization. In this scenario, τ sets the period of the coupled oscillation, and since $dK_c/d\tau < 0$, the coupling strength required to maintain synchronization increases with decreasing τ. Here, the synchronization we observed can be described as phase cohesiveness; the phases diverge until they are brought back together with a synchronizing pulse. If self-coupling is instead omitted from the network, following the same set of steps used

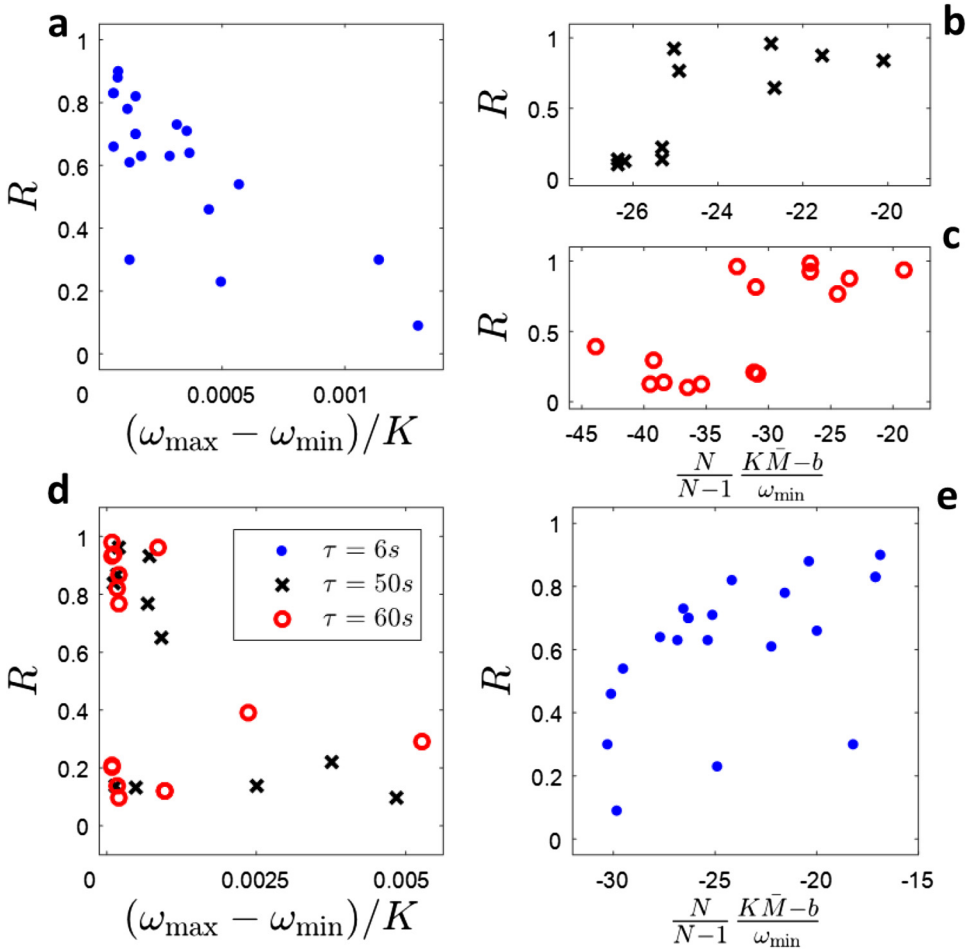

FIG. 7. (a) For $\tau = 6$ s, the spread in natural frequencies and the coupling strength provides the best prediction of synchronization in the network of oscillators. (b) and (c) For large values of τ, the coupling strength and minimum natural frequency are the best predictors of synchronization. (d) and (e) Plotting the order parameter against the opposite combination of parameters does not yield a clear pattern.

to derive Eq. (14) yields the critical coupling bound

$$K_c \leq NS_{max}[\tau\omega_{min}]/[\bar{M}(N-1)], \tag{15}$$

which only differs from Eq. (14) by a factor of $N/(N-1)$.

The important parameters that determine K_c in Eqs. (14) and (11) are quite different; for the former, the difference in natural frequencies is directly proportional to the upper bound on K_c; for the latter, the minimum natural frequency sets the bound, and the spread in natural frequencies is not important (τ, however, must still be smaller than the smallest natural period). As we will see, Eq. (14) provides a remarkably close estimate of the threshold required to maintain synchronization in a network of BZ oscillators.

IV. EVALUATION OF ANALYTICALLY DETERMINED BOUNDS FOR SYNCHRONIZATION

All experiments and simulations are performed with $N = 40$ oscillators. In simulations of Eq. (2), we take $q_i = 0.68 + (i-1)\frac{0.12}{39}$ with resulting natural periods $T \in [33.7, 38.5]$. Crosses in Fig. 6(a) represent the true value of K_c numerically determined by Eq. (2) by first taking K large enough so that the population is initially phase cohesive and slowly decrementing until phase cohesiveness is lost. When τ is between 10 and 20 time units, the population does not support phase cohesive solutions, even at large coupling strengths. The allowable heterogeneity of the iPRC, Figs. 1(b) and 1(c), is used to calculate β at various values of τ according to the strategy given in Appendix B, and this information is used to provide the bound for K_c in Eq. (11), shown as a solid black line in Fig. 6(a). The calculation of this bound assumes that the iPRC completely characterizes the spiking behavior of this system; however, this is not exactly true. Consider, for instance, oscillators that are lagging the most in a phase cohesive system when τ is relatively small. When the leading oscillators spike, τ time units later, the coupling felt by the lagging oscillators, which have yet to spike, ramps up quickly. Because the lagging oscillators are near the end of their cycle, this perturbation will generally be in excess of the threshold to elicit an immediate spike. Here, the effect of coupling is significantly underestimated for the lagging oscillators and we can remedy this situation with the approximation $\Gamma_{max}(\varphi_{i,j}) = -\infty$ when $\varphi_{i,j} < -(2\pi\tau)/T$. Note that when τ is small and the system is phase cohesive, the leading oscillators do not feel much coupling near the end of their cycle and do not have immediate spiking; therefore, we do not need to apply any corrections to Γ_{min}. We recalculate β with this new assumption on Γ_{max}, and the resulting upper bound is shown as the dashed line in Fig. 6(a). Equation (14) is used to estimate K_c at larger values of τ, shown as a dash-dotted line. Here, $\bar{M}$ is found numerically to be 0.9.

In Figs. 6(b) and 6(c), each cross represents a simulation of Eq. (2) with parameter $q_i = \nu\sigma_i + 0.74$, where σ_i is chosen from a standard normal distribution and ν varies

between 0 and 0.1 for each simulation. In the case that ν is large, q_i is further constrained to be between 0.68 and 0.8 (respectively, 0.5 and 0.87) in simulations in Fig. 6(b) [respectively, Fig. 6(c)], which sets the allowable amount of heterogeneity and ensures that each oscillator has a well-defined limit cycle. In each simulation, K is chosen between 0.2 and 2. Starting from an initial synchronous state, the order parameter, R, is recorded once the long-time behavior has been established. In Fig. 6(b), the vertical dashed line shows β calculated for $\tau = 6$ time units from Eq. (11) and we would expect all data points to the left to be phase cohesive. Closed (respectively, open) circles indicate simulations which remain phase cohesive (respectively, lose phase cohesiveness). The leftmost open circle occurs at a value only 14% larger than the dashed line threshold, indicating that the upper bound on the critical coupling strength is reasonably tight for these populations of oscillators. In Fig. 6(c), the vertical line corresponds to a cutoff for phase cohesiveness predicted by Eq. (14). In these simulations, however, some open circles occur slightly to the left of the cutoff. The reason for this discrepancy can likely be attributed to neglecting the effect of infinitesimal perturbations in Eq. (13), which have a small effect on the phase dynamics. Nevertheless, the analytical predictions agree quite well with the results of the numerical simulations.

Figure 7 shows an analogous set of experiments using the experimental system of photosensitive BZ chemical oscillators. In Fig. 7(a), we find that R qualitatively matches the results from the numerical system for smaller values of τ, i.e., gradually increasing as $\omega_{\max} - \omega_{\min}$ decreases and as K increases. For the experimental system, we approximate the STC with a piecewise linear fit to the measured data points shown in Fig. 5 and assume the STC among all oscillators is identical. In the regime with a negative slope, our fit is $S(\theta) = a\theta + b$, with coefficients $a = -0.53\,\mathrm{mW\,cm^{-2}\,rad^{-1}}$ and $b = 2.61\,\mathrm{mW\,cm^{-2}}$. Substituting this value for the STC into Eq. (15), the condition to maintain synchronization can be expressed as $(K\bar{M} - b)/\omega_{\min} > a\tau$. Figures 7(b) and 7(c) show the result of experiments with $\tau = 50\,\mathrm{s}$ and 60 s, respectively. We see a clear cutoff between systems with high and low order parameters in these experiments. These cutoff locations are very close to their predicted values of -27.0 and $-32.4\,\mathrm{mW\,cm^{-2}\cdot(rad/s)^{-1}}$ for $\tau = 50\,\mathrm{s}$ and 60 s, respectively. As expected, as τ increases, the threshold for synchronization shifts to values which require smaller coupling strengths. Figures 7(d) and 7(e) show similar data plotted against the other set of parameters. In contrast to the panels above, there is not a clear pattern when the opposite combination of parameters is plotted against the order parameter.

V. DISCUSSION AND CONCLUSION

Motivated by the understanding of synchronization in populations of coupled BZ oscillators, we have developed strategies for predicting and understanding synchronization in populations of all-to-all coupled heterogeneous limit cycle oscillators. For the first strategy, the effects of coupling are assumed to be small enough that the response to perturbations can be understood using an iPRC. Under these assumptions, the difference in natural frequencies among oscillators is a desynchronizing influence that must be overcome by strong enough phase difference coupling and is in qualitative agreement with other results for populations of Kuramoto oscillators.[41,47] The overall dispersion of the phases of the oscillators grows as coupling decreases until phase cohesiveness is ultimately lost. As a result, in Figs. 6(b) and 7(a), we observe that the order parameter varies relatively smoothly as the coupling strength decreases; once phase cohesiveness is lost, the population still remains relatively synchronized.

In the second strategy, we investigate the stability of phase cohesive solutions for stronger perturbations which result in near-immediate spikes. The development and use of an STC allows for the understanding of synchronization in this regime, for which the oscillator with the smallest natural frequency determines the coupling strength necessary to maintain phase cohesiveness. In simulations for which coupling tends to elicit spikes in an all-or-nothing fashion, populations either remain phase cohesive or are completely asynchronous [see, e.g., Figs. 6(c), 7(b), and 7(c)]. Intuitively, this behavior is due to the all-or-nothing spiking from the coupling; if synchronization is not maintained for some oscillators, the feedback signal will become less concentrated, decreasing its magnitude and causing other oscillators to lose synchronization. This process continues until the feedback signal is too weak to elicit immediate spikes in most oscillators.

We are unaware of the use of a phase dependent, all-or-nothing spike threshold curve in the literature and believe that such a strategy could be useful for predicting and understanding synchronization in periodically spiking systems. For instance, using this framework, we find that strong excitatory coupling in a population of BZ oscillators can have a synchronizing influence even though strategies often used under the weak coupling assumption[48–50] would predict desynchronization. While the analytical predictions given in this work assume that perturbations can be understood with either an iPRC (for weak perturbations) or an STC (for stronger perturbations), it is likely that both mechanisms work in tandem to synchronize populations of coupled BZ oscillators. In the context of the standard phase reduction, Eq. (6), the immediate spiking mechanism could be implemented with the additional constraint that $u(t)Z_i[\theta(t)] = 2\pi - \theta_i(t)$ when $u(t) > S_i(\theta)$, where $S(\theta)$ is the STC. Strategies that make use of the STC can be implemented without the need for considering additional variables in the reduction, and the development of analytical strategies which use both mechanisms could be of interest for obtaining tighter bounds for the critical coupling strength and for understanding more complicated population behavior, such as the emergence of chimera states.[21,26]

Our synchronization results pertain to only the stability of synchronized states; however, it would be of interest to adapt them for studying spontaneous synchronization for populations of oscillators that are not initially synchronized. Additionally, the methodology used here could be adapted to understand the stability of two-cluster solutions, which are often observed in populations of spiking oscillators,[22] and synchronization when oscillators are not coupled in an all-to-all manner.[51]

The results of this work primarily focus on synchronization in deterministic systems; however, it would be of

practical interest to extend these results to investigate synchronization of stochastic processes. Such applications arise, e.g., in cardiac pacemakers, where calcium-induced-calcium-release[52,53] plays an important role in the synchronization of stochastic ryanodine receptor openings. The authors of Ref. 1 showed that the magnitude of the calcium current generated from individual ryanodine receptor openings regulates synchronization of calcium release throughout a diffusively coupled network. The resulting synchronous release of calcium from sarcoplasmic reticulum leads to diastolic depolarization, subsequently activates L-type calcium currents, and ultimately results in a spontaneous action potential.[54–56] These synchronized calcium releases that occur during the diastolic interval have been referred to as the calcium clock[57] in cardiac pacemaking cells. While the strategies presented in the current work are not explicitly suited for application to stochastic processes, it is an intriguing possibility that they could be extended to understand and predict synchronization in these contexts.

Most results with applications to synchronization in populations of coupled oscillators rely on the approximation that perturbations are sufficiently weak so their effects can be understood with an iPRC. In addition to the significant reduction in complexity that phase reduction affords, this mathematical framework is useful because as the response to perturbations become larger, the effects on the phase can still be qualitatively understood using an iPRC, even if quantitative predictions may be slightly less accurate.[58,59] In fact, in many excitable biological systems, it is likely that immediate spikes in response to perturbations significantly contribute to synchronization. For instance, in neurons, provided a sufficiently long period of time has passed since the last action potential, perturbations that drive the transmembrane voltage above a threshold voltage produce action potentials.[60] Simple models of periodically firing neurons also have phase dependent spiking thresholds that can be visualized in terms of their voltage nullclines.[50] Such behaviors cannot be reproduced using iPRC techniques which assume that perturbations are sufficiently small that the state dynamics remain reasonably close to the unperturbed limit cycle. Immediate spiking is commonly observed in the experimental measurement of neural PRCs, where larger perturbations applied near the end of the cycle tend to produce immediate spikes.[61,62] This behavior is generally viewed as a nuisance, as it masks the actual shape of the iPRC and is generally ignored in analytical work; however, it is an actual feature of living neurons. It may be possible to quantify the tendency of neurons to fire in response to stronger perturbations in terms of a spike threshold curve. Note that for the experimental and numerical BZ oscillator system, the STC provides a phase dependent threshold perturbation necessary for the generation of an immediate spike. In other systems, the magnitude and duration of a stimulus may be important for determining conditions for an immediate spike to occur; however, such corrections will invariably increase the number of variables necessary to characterize the reduced system.

Given the accuracy we have found in the analytical predictions, the use of the STC as described in this work may represent a desirable trade-off between accuracy and complexity of the resulting reduction. The use of iPRCs together with STCs could provide a convenient framework for further understanding the behavior of coupled oscillators in situations where coupling is sufficiently large enough to elicit immediate spikes.

ACKNOWLEDGMENTS

Support for this work by National Science Foundation (NSF) Grants DMS-1602841 (D.W.), CMMI-1635542 (J.M.), and CHE-1565665 (K.S. and M.R.T.) is gratefully acknowledged.

APPENDIX A: PROOF OF SYNCHRONIZATION CONDITIONS USING INFINITESIMAL PHASE RESPONSE CURVES

A derivation of the statements from Sec. III A regarding synchronization among populations of limit cycle oscillators subject to weak, all-to-all connectivity with self coupling is given here. A proof of these statements also appears in Ref. 45. For convenience, we restate the conditions (I) and (II) from Sec. III A here: for some $\gamma \in (0, \pi)$

(I) For all i and j, $\min_{a\in[0,\gamma]}\left[\Gamma_i(a) - \Gamma_j(a-\gamma)\right] \geq (\omega_{\max} - \omega_{\min})/K$.
(II) For all i, there exists $\delta_i > 0$ such that when $-\gamma \leq \varphi \leq \gamma$, $\frac{d}{d\varphi}\Gamma_i(\varphi) > \delta_i$.

Conditions (I) and (II) are used in statements (i) and (ii), which give sufficient conditions for phase cohesiveness and frequency synchronization, respectively.

(i) Sufficient condition for phase cohesion. If condition (I) from Sec. III A is satisfied, then for some initial time t_0 for which $\max_{i,j}|\vartheta_i(t_0) - \vartheta_j(t_0)| \leq \gamma$, it follows that $|\vartheta_i(t) - \vartheta_j(t)| \leq \gamma$ for all $t > t_0$.

Proof: Suppose $\max_{i,j}|\vartheta_i(t_0) - \vartheta_j(t_0)| = \gamma$. Consider a subset of any two oscillators from the larger population ϑ_m and ϑ_n such that $\vartheta_m(t_0) - \vartheta_n(t_0) = \gamma$. Using Eq. (10), we may write

$$\dot{\vartheta}_m - \dot{\vartheta}_n = \Delta\omega_m - \Delta\omega_n - \frac{K}{N}\sum_{j=1}^{N}\left[\Gamma_m(\varphi_{m,j}) - \Gamma_n(\varphi_{n,j})\right]. \tag{A1}$$

For all j, we know that $\gamma = \varphi_{m,j}(t_0) - \varphi_{n,j}(t_0)$ so that Eq. (A1) becomes

$$\dot{\vartheta}_m - \dot{\vartheta}_n = \Delta\omega_m - \Delta\omega_n - \frac{K}{N}\sum_{j=1}^{N}\left[\Gamma_m(\varphi_{m,j}) - \Gamma_n(\varphi_{m,j} - \gamma)\right]. \tag{A2}$$

Using condition (I), we can provide an upper bound for Eq. (A1),

$$\dot{\vartheta}_m - \dot{\vartheta}_n \leq (\omega_{\max} - \omega_{\min}) - \frac{K}{N}\sum_{j=1}^{N}[(\omega_{\max} - \omega_{\min})/K]$$
$$= 0. \tag{A3}$$

Equation (A3) implies that the phase difference of any two oscillators cannot grow larger than γ; therefore, the maximum phase difference between any two oscillators is upper bounded by γ for $t > t_0$, which implies statement (i).

(ii) Sufficient condition for frequency synchronization. If conditions (I) and (II) from Sec. III A are satisfied, then for some initial time t_0 for which $\max_{i,j}|\vartheta_i(t_0) - \vartheta_j(t_0)| \leq \gamma$, the network equation (10) is exponentially frequency synchronized.

Proof: Suppose $\max_{i,j}|\vartheta_i(t_0) - \vartheta_j(t_0)| = \gamma$. From the above analysis, because (I) is satisfied, we know that the maximum phase difference between any two oscillators will be upper bounded by γ for all future time, i.e., the population is phase cohesive. Noting that we can write $\varphi_{i,j} = \vartheta_i - \vartheta_j$, we take the time derivative of Eq. (10)

$$\frac{d}{dt}\dot{\vartheta}_i = -\sum_{j=1}^{N} a_{i,j}(t)(\dot{\vartheta}_i - \dot{\vartheta}_j), \tag{A4}$$

where $a_{i,j}(t) = \frac{K}{N}\frac{d}{d\varphi}\Gamma_i(\varphi)|_{\vartheta_i(t)-\vartheta_j(t)}$. We can rewrite Eq. (A4) as a linear time-varying consensus algorithm

$$\frac{d}{dt}\dot{\vartheta} = L(t)\dot{\vartheta}, \tag{A5}$$

where $\vartheta = [\vartheta_1, \vartheta_2, \ldots, \vartheta_N]^T$ and L is a matrix with diagonal terms $L_{i,i}(t) = -\sum_{j\neq i}^{N} a_{i,j}(t)$ and off-diagonal terms $L_{i,j}(t) = a_{i,j}(t)$. Notice that the row sums of L are always equal to zero. From condition (II), we know that the off-diagonal terms, $a_{i,j}(t) > \frac{K}{N}\delta_i > 0$, are bounded and continuous functions of time. Furthermore, at each time instant, the matrix is fully populated so that, in the graph theoretical sense,[63] any node is reachable from any other node. We invoke Theorem 1 from Ref. 64 to conclude that all components $\frac{d}{dt}\dot{\vartheta}_i$ must exponentially approach the same value (i.e., they achieve consensus).

Toward contradiction, suppose that $\lim_{t\to\infty}\frac{d}{dt}\dot{\vartheta} \neq \vec{0}$, where $\vec{0}$ is an appropriately sized vector of zeros. Then when the population achieves consensus, for all i, $\dot{\vartheta}_i$ is unbounded in time. We know, however, from Eq. (10) that this is not possible since Γ_i is a bounded function so that $\dot{\vartheta}_i$ cannot be arbitrarily large. Therefore, when the population achieves consensus, $\frac{d}{dt}\dot{\vartheta} = \vec{0}$. Thus, for each i, $\dot{\vartheta}_i$ will approach a constant. Suppose that there exist some i and j such that $\lim_{t\to\infty}\dot{\vartheta}_i = \omega_i^*$ and $\lim_{t\to\infty}\dot{\vartheta}_j = \omega_j^*$ with $\omega_i^* \neq \omega_j^*$. If this is the case, then at some time t_1, $|\vartheta_i(t_1) - \vartheta_j(t_1)| = \pi$, which contradicts (I), thereby implying statement (ii).

APPENDIX B: PRACTICAL USE OF THE UPPER BOUND FOR DETERMINING CRITICAL COUPLING STRENGTH

If the infinitesimal phase response curves of every oscillator in a given population equation (8) are known, the averaged functions $\Gamma_i(\varphi_{i,j})$ can be calculated for every oscillator; in principle, the difference between Γ_i and Γ_j could be calculated for all combinations of i and j in order to calculate β from Eq. (11) and hence determine the upper bound on the critical coupling strength for phase cohesiveness. In practice, however, this becomes a computationally exhaustive task as the number of oscillators in the population grows larger. Furthermore, in many biological applications,[46] exact measurements of PRCs may be prohibitive. In these cases, we provide a strategy for testing conditions (I) and (II) when the phase response curves are allowed to exist in some predefined range. This approach eliminates the need for knowing individual phase response curves to determine an upper bound for K_c.

To begin, we allow for heterogeneity in the phase response curves of Eq. (8) by assuming $Z_i(\theta) \in [Z_{\min}(\theta), Z_{\max}(\theta)]$, where $Z_{\min}(\theta)$ and $Z_{\max}(\theta)$, respectively, represent the maximum and minimum values that any Z_i can take. We also let $Z_i(\theta) = \overline{Z}(\theta) + \Delta Z_i(\theta)$, where

$$\overline{Z}(\theta) = [Z_{\max}(\theta) + Z_{\min}(\theta)]/2,$$
$$\Delta Z_i(\theta) = Z_i(\theta) - \overline{Z}(\theta). \tag{B1}$$

We then rewrite Eq. (10) as follows:

$$\begin{aligned}
\dot{\vartheta}_i &= \Delta\omega_i - \frac{\epsilon K}{TN}\int_0^T \Bigg\{\sum_{j=1}^{N}\left[\overline{Z}(\varphi_{i,j}+\omega_o t) + \Delta Z_i(\varphi_{i,j}+\omega_o t)\right] \\
&\qquad \times f(\varphi_{i,j}+\omega_o t, \omega_o t)\Bigg\} dt \\
&= \Delta\omega_i - \frac{K}{N}\sum_{j=1}^{N}\underbrace{\frac{\epsilon}{T}\int_0^T\left\{\left[\overline{Z}(\varphi_{i,j}+\omega_o t) f(\varphi_{i,j}+\omega_o t, \omega_o t)\right]\right\}dt}_{\Gamma_i^{\text{common}}(\varphi_{i,j})} \\
&\quad - \frac{K}{N}\sum_{j=1}^{N}\underbrace{\frac{\epsilon}{T}\int_0^T\left[\Delta Z_i(\varphi_{i,j}+\omega_o t) f(\varphi_{i,j}+\omega_o t, \omega_o t)\right]dt}_{\Gamma_i^{\text{individual}}(\varphi_{i,j})} \\
&= \Delta\omega_i - \frac{K}{N}\sum_{j=1}^{N}\left[\Gamma_i^{\text{common}}(\varphi_{i,j}) + \Gamma_i^{\text{individual}}(\varphi_{i,j})\right] \\
&= \Delta\omega_i - \frac{K}{N}\sum_{j=1}^{N}\Gamma_i(\varphi_{i,j}).
\end{aligned} \tag{B2}$$

Here, Γ_i^{common} represents a phase difference coupling common to each oscillator, and $\Gamma_i^{\text{individual}}$ is a phase difference determined by the particular value of $Z_i(\theta_i)$. Note in the above formulation

$$\Gamma_i(\varphi_{i,j}) = \Gamma_i^{\text{common}}(\varphi_{i,j}) + \Gamma_i^{\text{individual}}(\varphi_{i,j}). \tag{B3}$$

From Eq. (B1), for any oscillator, $|\Delta Z_i(\theta)| \leq [Z_{\max}(\theta) - Z_{\min}(\theta)]/2 \equiv Z_d(\theta)$, giving the bound

$$\begin{aligned}
&-\frac{1}{T}\int_0^T\left[\left|Z_d(\varphi_{i,j}+\omega_o t) f(\varphi_{i,j}+\omega_o t, \omega_o t)\right|\right]dt \\
&\quad \leq \Gamma_i^{\text{individual}}(\varphi_{i,j}) \\
&\quad \leq \frac{1}{T}\int_0^T\left[\left|Z_d(\varphi_{i,j}+\omega_o t) f(\varphi_{i,j}+\omega_o t, \omega_o t)\right|\right]dt.
\end{aligned} \tag{B4}$$

Here, $\Gamma_i^{\text{common}}(\varphi_{i,j})$ is the same for all oscillators so that Eq. (B4) can be used to calculate upper and lower bounds on $\Gamma_{\max}(\varphi) = \max_i[\Gamma_i(\varphi)]$ and $\Gamma_{\min}(\varphi) = \min_i[\Gamma_i(\varphi)]$, the maximum and minimum possible coupling functions, respectively, for any oscillator in the population. Once $\Gamma_{\max}$ and $\Gamma_{\min}$ have been obtained, it is relatively straightforward to calculate β from Eq. (11) in order to determine the upper bound for phase cohesiveness.

If we also require a guarantee of frequency synchronization, condition (II) from Sec. III A mandates that the derivatives of the phase difference coupling must always be

positive and bounded away from zero. Similar to the strategy used above, we can take the derivative of Eq. (B3) to yield

$$\begin{aligned}\frac{d}{d\varphi}\Gamma_i(\varphi) &= \frac{1}{T}\int_0^T \Big\{ \left[\overline{Z}(\varphi+\omega_o t) f(\varphi+\omega_o t,\omega_o t)\right]' \\ &\quad + \Delta Z_i'(\varphi+\omega_o t) f(\varphi+\omega_o t,\omega_o t) \\ &\quad + \Delta Z_i(\varphi+\omega_o t) f'(\varphi+\omega_o t,\omega_o t)\Big\} dt \\ &\geq \frac{1}{T}\int_0^T \Big\{ \left[\overline{Z}(\varphi+\omega_o t) f(\varphi+\omega_o t,\omega_o t)\right]' \\ &\quad + \min\Big[\Delta Z_i'(\varphi+\omega_o t) f(\varphi+\omega_o t,\omega_o t) \\ &\quad + \Delta Z_i(\varphi+\omega_o t) f'(\varphi+\omega_o t,\omega_o t)\Big]\Big\} dt, \end{aligned} \tag{B5}$$

where $' \equiv d/d\varphi$. If we wish to guarantee that condition (II) holds, we can restrict γ to include only values for which $\frac{d}{d\varphi}\Gamma_i(\varphi)$ is guaranteed to be positive and bounded away from zero for $|\varphi| \leq \gamma$ for any oscillator in the population.

[1] A. V. Maltsev, V. A. Maltsev, M. Mikheev, L. A. Maltseva, S. G. Sirenko, E. G. Lakatta, and M. D. Stern, "Synchronization of stochastic Ca^{2+} release units creates a rhythmic Ca^{2+} clock in cardiac pacemaker cells," Biophys. J. **100**, 271–283 (2011).

[2] E. S. Maywood, A. B. Reddy, G. K. Y. Wong, J. S. O'Neill, J. A. O'Brien, D. G. McMahon, A. J. Harmar, H. Okamura, and M. H. Hastings, "Synchronization and maintenance of timekeeping in suprachiasmatic circadian clock cells by neuropeptidergic signaling," Curr. Biol. **16**, 599–605 (2006).

[3] T. Matsuo, S. Yamaguchi, S. Mitsui, A. Emi, F. Shimoda, and H. Okamura, "Control mechanism of the circadian clock for timing of cell division in vivo," Science **302**, 255–259 (2003).

[4] P. Jiruska, M. de Curtis, J. G. R. Jefferys, C. A. Schevon, S. J. Schiff, and K. Schindler, "Synchronization and desynchronization in epilepsy: Controversies and hypotheses," J. Physiol. **591**, 787–797 (2013).

[5] P. Brown, "Abnormal oscillatory synchronisation in the motor system leads to impaired movement," Curr. Opin. Neurobiol. **17**, 656–664 (2007).

[6] M. G. Pedersen, E. Mosekilde, K. S. Polonsky, and D. S. Luciani, "Complex patterns of metabolic and Ca^{2+} entrainment in pancreatic islets by oscillatory glucose," Biophys. J. **105**, 29–39 (2013).

[7] A. T. Winfree, "Biological rhythms and the behavior of populations of coupled oscillators," J. Theor. Biol. **16**, 15–42 (1967).

[8] Y. Kuramoto, *Chemical Oscillations, Waves, and Turbulence* (Springer-Verlag, Berlin, 1984).

[9] F. Dörfler and F. Bullo, "Synchronization in complex networks of phase oscillators: A survey," Automatica **50**, 1539–1564 (2014).

[10] L. M. Childs and S. H. Strogatz, "Stability diagram for the forced Kuramoto model," Chaos **18**, 043128 (2008).

[11] G. Filatrella, A. H. Nielsen, and N. F. Pedersen, "Analysis of a power grid using a Kuramoto-like model," Eur. Phys. J. B Condens. Matter Complex Syst. **61**, 485–491 (2008).

[12] Z. Lu, K. Klein-Cardeña, S. Lee, T. M. Antonsen, M. Girvan, and E. Ott, "Resynchronization of circadian oscillators and the east-west asymmetry of jet-lag," Chaos **26**, 094811 (2016).

[13] S. H. Strogatz, D. M. Abrams, A. McRobie, B. Eckhardt, and E. Ott, "Theoretical mechanics: Crowd synchrony on the millennium bridge," Nature **438**, 43–44 (2005).

[14] L. M. Pecora and T. L. Carroll, "Master stability functions for synchronized coupled systems," Phys. Rev. Lett. **80**, 2109 (1998).

[15] M. Dhamala, V. K. Jirsa, and M. Ding, "Enhancement of neural synchrony by time delay," Phys. Rev. Lett. **92**, 074104 (2004).

[16] W. Lohmiller and J. J. E. Slotine, "Control system design for mechanical systems using contraction theory," IEEE Trans. Automat. Contr. **45**, 984–989 (2000).

[17] W. Lohmiller and J. J. E. Slotine, "On contraction analysis for non-linear systems," Automatica **34**, 683–696 (1998).

[18] R. E. Mirollo and S. H. Strogatz, "Synchronization of pulse-coupled biological oscillators," SIAM J. Appl. Math. **50**, 1645–1662 (1990).

[19] M. Timme and F. Wolf, "The simplest problem in the collective dynamics of neural networks: Is synchrony stable?, Nonlinearity **21**, 1579 (2008).

[20] J. T. Ariaratnam and S. H. Strogatz, "Phase diagram for the Winfree model of coupled nonlinear oscillators," Phys. Rev. Lett. **86**, 4278 (2001).

[21] D. Pazó and E. Montbrió, "Low-dimensional dynamics of populations of pulse-coupled oscillators," Phys. Rev. X **4**, 011009 (2014).

[22] A. F. Taylor, P. Kapetanopoulos, B. J. Whitaker, R. Toth, L. Bull, and M. R. Tinsley, "Clusters and switchers in globally coupled photochemical oscillators," Phys. Rev. Lett. **100**, 214101 (2008).

[23] A. F. Taylor, P. Kapetanopoulos, B. J. Whitaker, R. Toth, L. Bull, and M. R. Tinsley, "Phase clustering in globally coupled photochemical oscillators," Eur. Phys. J. Spec. Top. **165**, 137–149 (2008).

[24] S. Nkomo, M. R. Tinsley, and K. Showalter, "Chimera states in populations of nonlocally coupled chemical oscillators," Phys. Rev. Lett. **110**, 244102 (2013).

[25] R. Snari, M. R. Tinsley, D. Wilson, S. Faramarzi, T. I. Netoff, J. Moehlis, and K. Showalter, "Desynchronization of stochastically synchronized chemical oscillators," Chaos **25**, 123116 (2015).

[26] S. Nkomo, M. R. Tinsley, and K. Showalter, "Chimera and chimera-like states in populations of nonlocally coupled homogeneous and heterogeneous chemical oscillators," Chaos **26**, 094826 (2016).

[27] E. M. Izhikevich, *Dynamical Systems in Neuroscience: The Geometry of Excitability and Bursting* (MIT Press, London, 2007).

[28] A. M. Zhabotinsky, F. Buchholtz, A. B. Kiyatkin, and I. R. Epstein, "Oscillations and waves in metal-ion-catalyzed bromate oscillating reactions in highly oxidized states," J. Phys. Chem. **97**, 7578–7584 (1993).

[29] A. E. Bugrim, M. Dolnik, A. M. Zhabotinsky, and I. R. Epstein, "Heterogeneous sources of target patterns in reaction-diffusion systems," J. Phys. Chem. **100**, 19017–19022 (1996).

[30] V. K. Vanag, L. F. Yang, M. Dolnik, A. M. Zhabotinsky, and I. R. Epstein, "Oscillatory cluster patterns in a homogeneous chemical system with global feedback," Nature **406**, 389–391 (2000).

[31] R. Toth, A. F. Taylor, and M. R. Tinsley, "Collective behavior of a population of chemically coupled oscillators," J. Phys. Chem. B **110**, 10170–10176 (2006).

[32] A. F. Taylor, M. R. Tinsley, F. Wang, Z. Y. Huang, and K. Showalter, "Dynamical quorum sensing and synchronization in large populations of chemical oscillators," Science **323**, 614–617 (2009).

[33] M. R. Tinsley, S. Nkomo, and K. Showalter, "Chimera and phase-cluster states in populations of coupled chemical oscillators," Nat. Phys. **8**, 662–665 (2012).

[34] H. Ke, M. R. Tinsley, A. Steele, F. Wang, and K. Showalter, "Link weight evolution in a network of coupled chemical oscillators," Phys. Rev. E **89**, 052712 (2014).

[35] J. F. Totz, R. Snari, D. Yengi, M. R. Tinsley, H. Engel, and K. Showalter, "Phase-lag synchronization in networks of coupled chemical oscillators," Phys. Rev. E **92**, 022819 (2015).

[36] T. R. Chen, M. R. Tinsley, E. Ott, and K. Showalter, "Echo behavior in large populations of chemical oscillators," Phys. Rev. X **6**, 041054 (2016).

[37] J. F. Totz, J. Rode, M. R. Tinsley, K. Showalter, and H. Engel, "Spiral wave chimera states in large populations of coupled chemical oscillators," Nat. Phys. **14**, 282–285 (2018).

[38] D. Yengi, M. R. Tinsley, and K. Showalter, "Autonomous cycling between excitatory and inhibitory coupling in photosensitive chemical oscillators," Chaos **28**, 045114 (2018).

[39] M. Salami, C. Itami, T. Tsumoto, and F. Kimura, "Change of conduction velocity by regional myelination yields constant latency irrespective of distance between thalamus and cortex," Proc. Natl. Acad. Sci. U.S.A. **100**, 6174–6179 (2003).

[40] E. M. Izhikevich, J. A. Gally, and G. M. Edelman, "Spike-timing dynamics of neuronal groups," Cereb. Cortex **14**, 933–944 (2004).

[41] F. Dörfler and F. Bullo, "On the critical coupling for Kuramoto oscillators," SIAM J. Appl. Dyn. Syst. **10**, 1070–1099 (2011).

[42] A. T. Winfree, *The Geometry of Biological Time*, 2nd ed. (Springer Verlag, New York, 2001).

[43] J. A. Sanders, F. Verhulst, and J. Murdock, *Averaging Methods in Nonlinear Dynamical Systems*, 2nd ed. (Springer-Verlag, New York, 2007).

[44] J. Guckenheimer and P. Holmes, *Nonlinear Oscillations, Dynamical Systems, and Bifurcations of Vector Fields* (Springer Verlag, New York, 1983), Vol. 42.

[45] D. Wilson and J. Moehlis, "Analytical bounds on the critical coupling strength in a population of heterogeneous biological oscillators," in *American Control Conference 2016* (IEEE, 2016), pp. 5772–5778.

[46]D. Wilson, A. B. Holt, T. I. Netoff, and J. Moehlis, "Optimal entrainment of heterogeneous noisy neurons," Front. Neurosci. **9**, 192 (2015).
[47]N. Chopra and M. W. Spong, "On exponential synchronization of Kuramoto oscillators," IEEE Trans. Automat. Contr. **54**, 353–357 (2009).
[48]C. Van Vreeswijk, L. F. Abbott, and G. B. Ermentrout, "When inhibition not excitation synchronizes neural firing," J. Comput. Neurosci. **1**, 313–321 (1994).
[49]D. Hansel, G. Mato, and C. Meunier, "Synchrony in excitatory neural networks," Neural. Comput. **7**, 307–337 (1995).
[50]G. B. Ermentrout and D. H. Terman, *Mathematical Foundations of Neuroscience* (Springer, New York, 2010).
[51]F. Dörfler, M. Chertkov, and F. Bullo, "Synchronization in complex oscillator networks and smart grids," Proc. Natl. Acad. Sci. U.S.A. **110**, 2005–2010 (2013).
[52]A. Fabiato and F. Fabiato, "Excitation-contraction coupling of isolated cardiac fibers with disrupted or closed sarcolemmas: Calcium-dependent cyclic and tonic contractions," Circ. Res. **31**, 293–307 (1972).
[53]A. Fabiato and F. Fabiato, "Calcium-induced release of calcium from the sarcoplasmic reticulum of skinned cells from adult human, dog, cat, rabbit, rat, and frog hearts and from fetal and new-born rat ventricles," Ann. N. Y. Acad. Sci. **307**, 491–522 (1978).
[54]J. Hüser, L. A. Blatter, and S. L. Lipsius, "Intracellular Ca^{2+} release contributes to automaticity in cat atrial pacemaker cells," J. Physiol. **524**, 415–422 (2000).
[55]K. Y. Bogdanov, T. M. Vinogradova, and E. G. Lakatta, "Sinoatrial nodal cell ryanodine receptor and Na^{+}-Ca^{2+} exchanger: Molecular partners in pacemaker regulation," Circ. Res. **88**, 1254–1258 (2001).
[56]V. A. Maltsev and E. G. Lakatta, "Synergism of coupled subsarcolemmal Ca2+ clocks and sarcolemmal voltage clocks confers robust and flexible pacemaker function in a novel pacemaker cell model," Am. J. Physiol. Heart Circ. Physiol. **296**, H594–H615 (2009).
[57]E. G. Lakatta, V. A. Maltsev, and T. M. Vinogradova, "A coupled SYSTEM of intracellular Ca^{2+} clocks and surface membrane voltage clocks controls the timekeeping mechanism of the heart's pacemaker," Circ. Res. **106**, 659–673 (2010).
[58]A. Zlotnik and J. S. Li, "Optimal entrainment of neural oscillator ensembles," J. Neural Eng. **9**, 046015 (2012).
[59]J. Moehlis, E. Shea-Brown, and H. Rabitz, "Optimal inputs for phase models of spiking neurons," ASME J. Comput. Nonlinear Dyn. **1**, 358–367 (2006).
[60]B. P. Bean, "The action potential in mammalian central neurons," Nat. Rev. Neurosci. **8**, 451 (2007).
[61]T. Netoff, M. A. Schwemmer, and T. J. Lewis, "Experimentally estimating phase response curves of neurons: Theoretical and practical issues," in *Phase Response Curves in Neuroscience* (Springer, New York, 2012), pp. 95–129.
[62]A. Nabi, T. Stigen, J. Moehlis, and T. Netoff, "Minimum energy control for *in vitro* neurons," J. Neural Eng. **10**, 036005 (2013).
[63]F. Bullo, J. Cortés, and S. Martinez, *Distributed Control of Robotic Networks: A Mathematical Approach to Motion Coordination Algorithms* (Princeton University Press, Princeton, NJ, 2009).
[64]L. Moreau, "Stability of continuous-time distributed consensus algorithms," in *43rd IEEE Conference on Decision and Control, 2004 (CDC)* (IEEE, 2004), Vol. 4, pp. 3998–4003.